Geological Magazine

www.cambridge.org/geo

Nd–Sr–Pb isotopes systematics of the Jurassic Evros ophiolite, eastern Circum-Rhodope Belt, NE Greece

Nikolay Bonev[1], Zornitsa Dotseva[1] and Massimo Chiaradia[2]

[1]Department of Geology, Paleontology and Fossil Fuels, Sofia University St Kliment Ohridski, BG-1504 Sofia, Bulgaria and [2]Department of Earth Sciences, University of Geneva, CH-1205 Geneva, Switzerland

Rapid Communication

Cite this article: Bonev N, Dotseva Z, and Chiaradia M (2023) Nd–Sr–Pb isotopes systematics of the Jurassic Evros ophiolite, eastern Circum-Rhodope Belt, NE Greece. *Geological Magazine* **160**: 198–205. https://doi.org/10.1017/S0016756822001285

Received: 28 June 2022
Revised: 8 December 2022
Accepted: 8 December 2022
First published online: 30 January 2023

Keywords:
whole-rock Nd–Sr–Pb isotopes; Evros ophiolite; Circum-Rhodope Belt; Greece

Author for correspondence:
Nikolay Bonev,
Email: niki@gea.uni-sofia.bg

Abstract

We report on the isotopic compositions of the Jurassic supra-subduction zone Evros ophiolite mafic rocks exposed in the eastern Circum-Rhodope Belt of northeastern Greece. These mafic units consist of low-Ti gabbroic and basaltic rocks, whose Nd–Sr–Pb isotopes are compatible with dominant mantle-derived MORB component mixed with a detectable amount of crustal material and/or sediment invoved in their melt source in the subduction zone. These isotopic features are consistent with an intra-oceanic arc origin of the mafic ophiolite rocks, and the Evros ophiolite Nd and Pb isotopes are comparable to those of the counterpart mafic rocks from the Mandritsa unit in Bulgaria.

1. Introduction

The Serbo-Macedonian and Rhodope high-grade metamorphic massifs constitute the crystalline basement of the Alpine orogenic belt in the Balkan Peninsula and display a record of a late Mesozoic convergence resulting in nappe stacking overprinted by an early Cenozoic extensional deformation (e.g. Burg *et al.* 1996; Bonev *et al.* 2006; Bonev & Beccaletto, 2007). Both massifs are surrounded by a very low- to low-grade Circum-Rhodope Belt (CRB) that extends from the Chalkidiki Penisula (western part) across the Aegean Sea to the Thrace area (eastern part) in northern Greece (Fig. 1; Kauffmann *et al.* 1976). The eastern CRB contains unmetamorphosed Evros ophiolite of supra-subduction zone origin (e.g. Magganas *et al.* 1991; Magganas, 2002; Bonev & Stampfli, 2008, 2009), which has Early–Middle Jurassic crystallization ages (Bonev *et al.* 2015*a*). The south-vergent, thrust system of the Serbo-Macedonian and Rhodope massifs was constructed during a contractional phase in the hanging wall of a north-dipping Cretaceous–Tertiary subduction zone that was located within Vardar Ocean further to the SSW (in the present-day coordinate system) (Ricou *et al.* 1998). However, the late Mesozoic shortening and nappe-stacking event was predated by intra-oceanic subduction that resulted in the formation of arc-related Evros ophiolite, which together with the associated sedimentary rocks was thrusted and accreted to the Serbo-Macedonian – Rhodope continental margin of Eurasia (Bonev & Stampfli, 2003, 2011; Bonev *et al.* 2010*a*, 2015*a*).

The low-grade metamorphic CRB forms the uppermost crustal unit of the Serbo-Macedonian and Rhodope massifs, with distinct metamorphic grade and N-directed kinematics compared to the high-grade basement (Bonev *et al.* 2010*a*; Bonev & Stampfli, 2011; Bonev & Filipov, 2018), which indicate that they all experienced a deformational event, and that they were already part of the crustal architecture in the Balkan Peninsula by the earliest Cretaceous (Ivanova *et al.* 2015; Bonev *et al.* 2015*a*, *b*). However, the nature of the CRB ophiolite melt source(s) is not well understood. The existing models consider them as ophiolitic allochthonous tectonic sheets, representing the remnants of a Tethyan oceanic lithosphere (Robertson *et al.* 1996; Robertson, 2002; Papanikolaou, 2009; Stampfli & Hochard, 2009; Bonev *et al.* 2010*a*, 2015*a*, *b*; Ferrière *et al.* 2016), which formed in fore-arc, intra-arc/arc and back-arc environments (Bonev & Stampfli, 2008, 2009; Bonev *et al.* 2010*b*, 2015*a*, *b*; Bonev, 2020). These different arc-related settings have major implications for the crustal evolution of the Balkan Peninsula and need to be validated with isotopic studies.

In this paper, we report on the Nd–Sr–Pb radiogenic isotope geochemistry of the Evros ophiolite mafic units in the eastern CRB exposed in northeastern Greece (Fig. 1). Our isotopic data suggest crust–mantle interaction recorded in these mafic rock units, which represent island arc magmatic assemblages formed during intra-oceanic subduction evolution outboard the Rhodope margin in the Early to Late Jurassic. We present a brief account of the regional geology, geochemistry and isotopic signature of the Jurassic Evros ophiolite mafic rocks, and then discuss their origin in different arc-related magmatic settings.

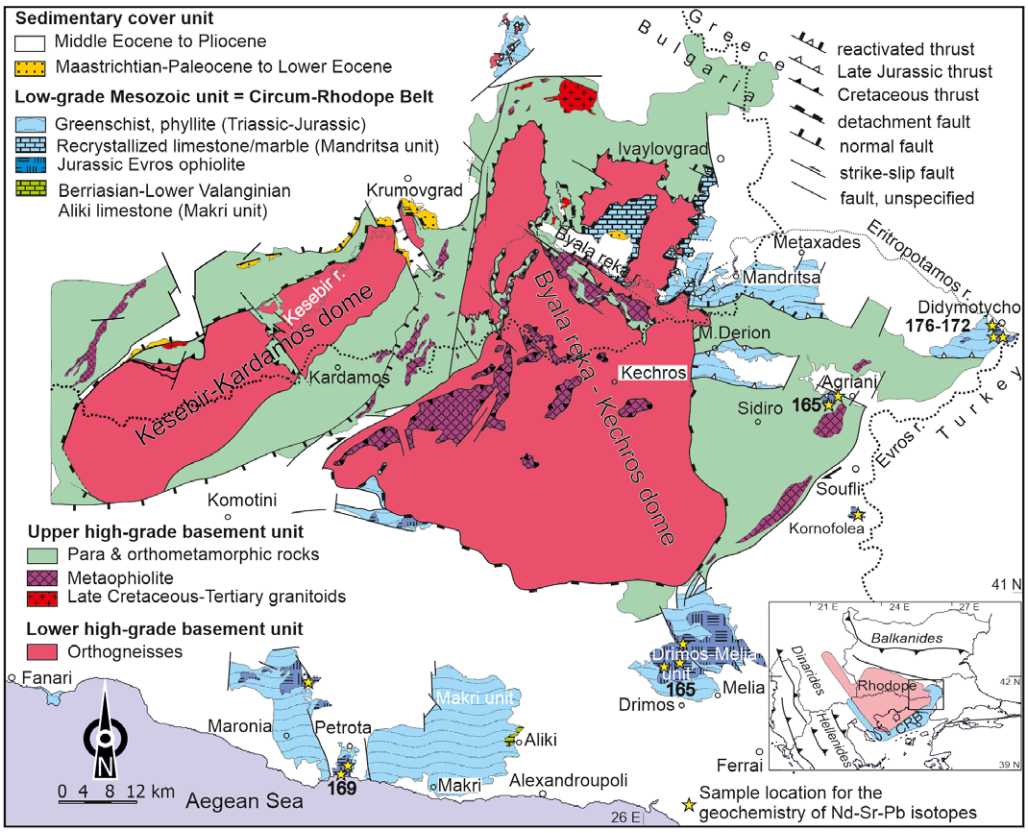

Fig. 1. (Colour online) Simplified geological map of the eastern Rhodope Massif in southern Bulgaria and northern Greece (after Bonev *et al.* 2015*a*), showing the locations of studied samples listed in Table 1. Bold numbers refer to radiometric ages of the Evros ophiolite. Inset: tectonic framework of the Alpine system in the Aegean domain of the eastern Mediterranean region.

2. Regional geology of the eastern CRB and Evros ophiolite

In the Thrace area of the northern Aegean region, the Evros ophiolite is exposed from the Aegean coast in Greece up to the northern tip of the eastern Rhodope Massif in Bulgaria, and built the eastern CRB, also called the Mesozoic low-grade unit (Fig. 1, inset; e.g. Bonev & Stampfli, 2003). The Samothraki Island is an extension of the Evros ophiolite offshore Greece, named Samothraki ophiolite of back-arc origin (Tsikuras & Hatzipanagiotou, 1998). The two main units of the eastern CRB include the greenschist-facies metasedimentary Makri unit and the overlying very low-grade to unmetamorphosed Drimos–Melia unit; the latter in turn includes a major part of the Evros ophiolite (Fig. 1; Papadopoulos, 1980, 1982). The eastern CRB overlies the upper unit of the high-grade basement with a reworked thrust contact and by extensional detachments directly onto the lower unit of the high-grade basement testifying for extensional omissions in the tectonostratigraphy (Fig. 1; Bonev & Stampfli, 2011).

The Makri unit consists of stratigraphically lower metasedimentary series conformably overlain by an upper metavolcanic–sedimentary series, which are intercalated with two marble horizons and covered by a single limestone horizon. The metasedimentary series (i.e. marble–shale–phyllite sequences) has the characteristics of shallow-marine platform type slope-rise deposits (Papadopoulos *et al.* 1989). One of the lowest marble horizons yielded Upper Triassic corals (Maratos & Andronopoulos, 1964), and the metasedimentary series supplied Tithonian–Beriassian ammonites (Dimadis & Nikolov, 1997). The youngest group of detrital zircons in the sandstones cluster at *c.* 240 Ma, providing at least a Middle Triassic depositional age for the stratigraphically lower levels of the Makri unit (Meinhold *et al.* 2010). The metavolcanic–sedimentary series is dominated by greenschists derived from mafic to acid lavas and pyroclastics, with occurrences of scarce serpentinite bodies. The uppermost limestone horizon, known as Lower Cretaceous 'Aliki limestones' (Maratos & Andronopoulos, 1964), lies unconformably on the metavolcanic–sedimentary series (Kopp, 1969; Ivanova *et al.* 2015), implying a pre-Cretaceous age of deposition and greenschist-facies metamorphism of the Makri unit. Recent biostratigraphic data confirmed Beriassian – lower Valanginian depositional age of the 'Aliki limestones' (Ivanova *et al.* 2015).

The Drimos–Melia unit consists of massive mafic lava flows intruded by mafic dykes and pillow lavas of the Evros ophiolite intercalated in a flysch succession (Papadopoulos, 1982; Papadopoulos *et al.* 1989; Bonev & Stampfli, 2005; Bonev, 2020), which yielded Middle–Upper Triassic (Dimadis *et al.* 1996) and Middle–Upper Jurassic (Trikkalinos, 1955) biostratigraphic ages. The detrital zircons in the flysch cluster at *c.* 315–285 Ma, and the youngest grain at *c.* 160 Ma provides a Late Jurassic maximum age of deposition (Meinhold *et al.* 2010).

Middle Eocene to Oligocene sedimentary rocks represents unconformable sedimentary cover unit onto the Makri and Drimos–Melia units, which includes also thick Late Eocene – Oligocene up to early Miocene volcanic and volcanic–sedimentary successions (Kopp, 1965; Christofides *et al.* 2004).

The Evros ophiolite consists of massive and rare pillow tholeiitic basalt, and evolved boninitic–tholeiitic basaltic andesite–andesite lavas (e.g. Magganas *et al.* 1991; Magganas, 2002; Bonev & Stampfli, 2005, 2008), together with tholeiitic to calc-alkaline cumulitic and isotropic gabbro (Biggazzi *et al.* 1989; Bonev & Stampfli, 2009), which together demonstrate a typical upper crustal intrusive and volcanic section of an ophiolite. Volcanic section of

https://doi.org/10.1017/S0016756822001285 Published online by Cambridge University Press

the Evros ophiolite is most extensively exposed in the Drimos–Melia unit, but other smaller exposures also occur at the villages of Krovili and Kornofolea and at the town of Didymotycho (Fig. 1). One of the intrusive members of the Evros ophiolite, called the Petrota gabbroic complex (Biggazzi *et al.* 1989), is exposed within the Tertiary Petrota graben. According to U–Pb zircon dating, the Petrota gabbro crystallized at 169 ± 2 Ma (Koglin *et al.* 2007), and apatite fission-track ages ranging between 161 Ma and 140 Ma (Biggazzi *et al.* 1989) from the gabbro reveal the shallow crustal low-temperature history. Another Evros ophiolite intrusive section gabbroic body occurs at the village of Agriani (Bonev & Stampfli, 2009). At Agriani, an isotropic gabbro is cross-cut by boninitic dykes, and the gabbro yielded a $^{40}Ar/^{39}Ar$ amphibole cooling age of 163.49 ± 3.85 Ma (Bonev *et al.* 2015*a*). Further east at the town of Didymotycho, a plagiogranite stock is cross-cut by boninitic–tholeiitic basalt and andesite dykes (Bonev & Stampfli, 2009). Rare-earth element modelling suggests that the plagiogranite is the result of extreme fractional crystallization of a basaltic magma similar in composition to the dykes intruding the plagiogranite. At Didymotycho, according to U–Pb zircon dating, the 171 Ma old plagiogranite intruded into 176 Ma old gabbro as well as into massive tholeiitic basalt lavas overlying the gabbro (Bonev *et al.* 2015*a*). Bonev & Stampfli (2009) have interpreted the Evros ophiolite occurrences at Agriani and Didymotycho as a proto-arc (fore-arc) segment of the large-scale eastern Rhodope – Evros Jurassic intra-oceanic arc system. Equivalent to the Evros ophiolite, the low-K and low-Ti boninitic–tholeiitic massive lavas are included in the Mandritsa unit in Bulgaria, from which Nd ($^{143}Nd/^{144}Nd_i = 0.512405–0.512950$) and Pb ($^{206}Pb/^{204}Pb_i = 18.132–18.564$; $^{207}Pb/^{204}Pb_i = 15.573–15.640$; $^{208}Pb/^{204}Pb_i = 37.959–38.551$) isotopes are available (Bonev & Stampfli, 2008). Collectively, based on geochemical affinities, the Evros ophiolite generated in fore-arc to arc tectonic environments, and it can be classified as subduction-related supra-subduction type to volcanic arc type ophiolite (e.g. Dilek & Furnes, 2011).

3. Nd–Sr–Pb isotopes results

We analysed three samples from the mafic rocks at Didymotycho (GR59, GR46-9, Dd2) and three samples from the Drimos–Melia unit (GR11-73, GR41-9, GR35-9), together with two samples from the Agriani (AGR, GR11-65) and three samples from the Petrota (GR53-9, GR12-9, GR24-9) gabbroic bodies, and a mafic rock sample (GR44-9) at the village of Kornofolea for Nd, Sr and Pb isotopic compositions (Fig. 1; Table 1). Whole-rock compositions of these samples are published in Bonev & Stampfli (2009), Bonev *et al.* (2015*a*) and Bonev (2020). We compared the Nd and Pb isotopes of our rock samples to the published Nd and Pb isotopic compositions of the mafic ophiolitic rocks in the adjacent Mandritsa unit of the CRB, in Bulgaria (Bonev & Stampfli, 2008).

Chemical separation of the samples and whole-rock isotopic analyses were done in the Department of Earth Sciences at the University of Geneva (Switzerland) and calibrated against both international and internal standards. Nd–Sr–Pb isotopes were measured on a Thermo Neptune PLUS Multi-Collector inductively coupled plasma – mass spectrometer (ICP-MS). For monitoring the internal fractionation, we used $^{88}Sr/^{86}Sr = 8.375209$ for the $^{87}Sr/^{86}Sr$ ratio, $^{146}Nd/^{144}Nd = 0.7219$ for the $^{143}Nd/^{144}Nd$ ratio and $^{203}Tl/^{205}Tl = 0.418922$ for the three Pb ratios. Long-term reproducibility of the measurements was controlled by repeated measurements of the external standards SRM987 ($^{87}Sr/^{86}Sr = 0.710248$, McArthur *et al.* 2001; JNdi-1 $^{143}Nd/^{144}Nd = 0.512115$, Tanaka *et al.* 2000) and SRM981 (Baker *et al.* 2004) for Pb. Further analytical details can be found in Chiaradia *et al.* (2011). The whole-rock Nd, Sr and Pb isotopic compositions are given in Tables 2-4. The Nd–Sr–Pb isotopic results were age-corrected to the known crystallization ages of the Evros ophiolite or biostratigraphic age of the sediments associated to this ophiolite (see Table 1).

The $^{143}Nd/^{144}Nd$ ratios of the mafic rock samples fall in the range 0.512571–0.512976, with positive ϵ_{Nd} values that are characteristic of mantle melts, and only a single exception of sample GR44-9 with negative $\epsilon_{Nd} = -1.3$. When time-corrected for the crystallization age of the mafic rocks (176 Ma to 165 Ma; see Table 1), the $\epsilon_{Nd}(t)$ values vary from +0.2 to +6.6 (Table 3). The $^{87}Sr/^{86}Sr$ ratios display values ranging from 0.703998 to 0.707584 that are characteristic of the oceanic crust and subduction-related volcanic rocks (Table 2). However, basalt sample GR44-9 at Kornofolea and sample Dd2 from the dyke at Didymotycho have higher $^{87}Sr/^{86}Sr$ ratios of 0.707153 and 0.707584, respectively. These data indicate that the analysed mafic rocks except samples GR44-9 and Dd2 originated from magmas that were derived from a similar mantle source with a high time-integrated Sm/Nd ratio and with a moderate range of Rb/Sr ratios. In a correlative $^{143}Nd/^{144}Nd$ vs $^{87}Sr/^{86}Sr$ diagram (Fig. 2a), the majority of the samples parallel the mantle array and plot close to the Bulk Silica Earth (BSE), while samples GR41-9 and GR44-9 plot close to BSE and sample Dd2 plots with high $^{87}Sr/^{86}Sr$ ratio. In a $^{143}Nd/^{144}Nd$ vs $^{206}Pb/^{204}Pb$ diagram isotopic ratios cluster between the BSE, Prevalent Mantle (PREMA) and Mid-Ocean Ridge Basalt (MORB) (Fig. 2b) and spread along the same mantle reservoirs towards higher $^{87}Sr/^{86}Sr$ ratios in the $^{87}Sr/^{86}Sr$ vs $^{206}Pb/^{204}Pb$ diagram (Fig. 2c).

The $^{206}Pb/^{204}Pb$ ratios of the analysed rocks show a relatively narrow range (18.314–18.930), display a narrow range of $^{207}Pb/^{204}Pb$ ratios (15.565–15.670) and a relatively narrow range of $^{208}Pb/^{204}Pb$ ratios (38.197–39.096), reaching a higher value in sample GR53-9 (Table 4). Almost all the mafic rocks exhibit a short linear trend parallel to progressive enrichment along the MORB–OIB line in the $^{207}Pb/^{204}Pb$–$^{206}Pb/^{204}Pb$ correlation diagram (Fig. 2d), plotting above the Northern Hemisphere Reference Line (NHRL) where enriched mantle reservoirs (EMI, EMII) are identified (Zindler & Hart, 1986). An exception of Pb isotopic compositions is a single sample plotting within the large OIB field and close to the MORB field (Rollinson, 1993). In a $\epsilon_{Nd}(t)$ vs $^{206}Pb/^{204}Pb$ diagram samples show linear trend toward higher $\epsilon_{Nd}(t)$ values plotting between the MORB and the BSE (Fig. 2e).

The analysed Evros ophiolite mafic rock samples have Pb isotope ratios that cluster close to those of the counterpart Jurassic mafic rocks (lavas and greenschists) from the Mandritsa unit of the CRB in Bulgaria, which in turn partly plot within the OIB field (closest to the MORB field) (Bonev & Stampfli, 2008). However, our samples from the Evros ophiolite show high $^{206}Pb/^{204}Pb$ and $^{207}Pb/^{204}Pb$ ratios. When the Mandritsa unit mafic rocks are compared to our Evros ophiolite samples, both rock suites display striking similarities in terms of Nd–Pb isotopic compositions (Fig. 2d, e).

4. Discussion and conclusions

The Nd isotope compositions obtained in this study are consistent with involvement of MORB reservoir, a compositional feature also displayed by trace element and REE geochemistry of the studied

https://doi.org/10.1017/S0016756822001285 Published online by Cambridge University Press

Table 1. Summary of studied samples from the Evros ophiolite. Location of samples is shown in Figure 1

Sample	Rock type	Remark	Age	Reference for whole-rock composition	Location
GR59	Basalt	Massive, overlying Dydimotycho gabbro and intruded by Dydimotycho plagiogranite dated at 171.9 ± 1.5 Ma (U–Pb zircon)	172 Ma	Bonev, 2020	Dydimotycho
GR46-9	Gabbro	Isotropic, intruded by Dydimotycho plagiogranite	U–Pb zircon age 176.4 ± 0.93 Ma Bonev *et al.* 2015*a*	Bonev *et al.* 2015*a*	Dydimotycho
Dd2	Basalt	Dyke intruding Dydimotycho plagiogranite	170 Ma	Bonev & Stampfli, 2009	Dydimotycho
GR44-9	Basalt	Massive	165 Ma Age based on regional setting close to the Drimos–Melia unit	Bonev, 2020	Kornofolea
AGR	Gabbro	Isotropic	163.49 ± 3.85 Ma $^{40}Ar/^{39}Ar$ amphibole age Bonev *et al.* 2015*a*	Bonev & Stampfli, 2009	Agriani
GR11-65	Basalt	Massive, overlying Agriani gabbro	164 Ma	Bonev, 2020	Agriani
GR53-9	Gabbro	Isotropic	U–Pb zircon age 169 ± 2 Ma Koglin *et al.* 2007	Bonev, 2020	Petrota
GR12-9	Basalt	Massive	169 Ma Age based on regional setting close to the Petrota gabbro	Bonev, 2020	Krovili
GR24-9	Anorthosite	Dyke, mutually intrusive into Petrota gabbro	169 Ma	Bonev, 2020	Petrota
GR11-73	Basalt	Dyke	165 Ma biostratigraphic age after Trikkalinos, 1955	Bonev, 2020	Drimos–Melia unit
GR41-9	Basaltic andesite	Pillowed	165 Ma biostratigraphic age after Trikkalinos, 1955	Bonev, 2020	Drimos–Melia unit
GR-35-9	Andesite	Massive	165 Ma biostratigraphic age after Trikkalinos, 1955	Bonev, 2020	Drimos–Melia unit

Table 2. Sr isotopic compositions of the Evros ophiolite mafic rocks

Sample	High	$^{87}Sr/^{86}Sr$ new slit	1SE	Signal	FC $^{87}Sr/^{86}Sr$ new slit*	1,00002	Factor	ppm 1 sigma	1 sigma recalculated ppm (external uncertainty)
GR59	0.704814	0.704807	0.000007	1.51	0.704793		20	0.001956354	0.000014
GR46-9	0.704016	0.704012	0.000004	5.72	0.703998		9	0.00085077	0.000006
Dd2	0.707614	0.707598	0.000016	0.63	0.707584		34	0.00337736	0.000024
GR44-9	0.707174	0.707167	0.000007	1.78	0.707153		18	0.001765934	0.000012
AGR	0.704676	0.704673	0.000003	4.89	0.704659		9	0.000938908	0.000007
GR11-65	0.704607	0.704603	0.000004	3.81	0.704589		11	0.001097988	0.000008
GR53-9	0.704281	0.704278	0.000003	5.36	0.704264		9	0.000886022	0.000006
GR12-9	0.705644	0.705636	0.000008	1.51	0.705622		20	0.001955902	0.000014
GR24-9	0.705012	0.705009	0.000003	6.52	0.704995		8	0.000783748	0.000006
GR11-73	0.704170	0.704167	0.000003	9.15	0.704153		6	0.0006344	0.000004
GR41-9	0.706559	0.706554	0.000005	2.64	0.706540		14	0.00138043	0.000010
GR35-9	0.705341	0.705335	0.000006	1.86	0.705321		17	0.001719985	0.000012

*Values corrected for internal fractionation using $^{88}Sr/^{86}Sr = 8.375209$ and for external fractionation using a nominal value of SRM987 $^{87}Sr/^{86}Sr = 0.710248$ (McArthur *et al.* 2001).

https://doi.org/10.1017/S0016756822001285 Published online by Cambridge University Press

Table 3. Nd isotopic compositions of the Evros ophiolite mafic rocks

Sample	Low	High	^{143}Nd/^{144}Nd	1 SE	Epsilon CHUR	FC ^{143}Nd/^{144}Nd*	Factor	0.999951	^{140}Ce	Signal ^{144}Nd
GR59	0.512851	0.512857	0.512854	0.000003	4.7	0.512879			1.325	1.275
GR46-9	0.512949	0.512953	0.512951	0.000002	6.6	0.512976			3.204	2.136
Dd2	0.512937	0.512940	0.512939	0.000002	6.4	0.512964			1.627	2.143
GR44-9	0.512543	0.512550	0.512546	0.000004	−1.3	0.512571			1.113	0.808
AGR	0.512844	0.512855	0.512850	0.000006	4.6	0.512875			0.543	0.327
GR11-65	0.512885	0.512891	0.512888	0.000003	5.4	0.512913			1.876	1.089
GR53-9	0.512818	0.512822	0.512820	0.000002	4.0	0.512845			3.341	1.637
GR12-9	0.512868	0.512875	0.512872	0.000003	5.0	0.512897			2.181	0.854
GR24-9	0.512694	0.512738	0.512716	0.000022	2.0	0.512741			0.192	0.056
GR11-73	0.512872	0.512876	0.512874	0.000002	5.1	0.512899			4.404	3.085
GR41-9	0.512620	0.512628	0.512624	0.000004	0.2	0.512649			1.043	0.544
GR35-9	0.512778	0.512783	0.512780	0.000002	3.3	0.512805			4.565	1.442

*Values corrected for internal fractionation using ^{146}Nd/^{144}Nd = 0.7219 and for external fractionation using a nominal value of JNdi1 ^{143}Nd/^{144}Nd = 0.512115 (Tanaka *et al.* 2000).

Table 4. Pb isotopic compositions of the Evros ophiolite mafic rocks

Sample	^{205}Tl	^{208}Pb	^{206}Pb/^{204}Pb	^{207}Pb/^{204}Pb	^{208}Pb/^{204}Pb	1SE 6/4	1SE 7/4	1SE 8/4	^{206}Pb/^{204}Pb*FC	^{207}Pb/^{204}Pb*FC	^{208}Pb/^{204}Pb*FC
GR59	2.06	1.15	18.6457	15.6436	38.7467	0.0008	0.0006	0.0016	18.659	15.661	38.803
GR46-9	2.14	0.08	18.4804	15.6123	38.6120	0.0093	0.0077	0.0192	18.494	15.629	38.668
Dd2	2.14	0.35	18.6663	15.6214	38.7433	0.0020	0.0017	0.0043	18.680	15.638	38.800
GR44-9	2.18	0.40	18.4593	15.6010	38.4400	0.0018	0.0015	0.0037	18.473	15.618	38.496
AGR	2.15	2.84	18.6351	15.6533	38.7707	0.0003	0.0003	0.0008	18.649	15.670	38.827
GR11-65	2.16	0.11	18.8639	15.5476	38.6279	0.0055	0.0045	0.0114	18.878	15.565	38.684
GR53-9	2.21	0.46	18.9158	15.6465	39.0390	0.0018	0.0014	0.0036	18.930	15.664	39.096
GR12-9	2.12	0.26	18.4437	15.6015	38.3598	0.0023	0.0020	0.0047	18.457	15.619	38.416
GR24-9	2.06	0.10	18.3005	15.5583	38.1414	0.0063	0.0054	0.0129	18.314	15.575	38.197
GR11-73	2.04	0.36	18.5518	15.6028	38.4901	0.0019	0.0016	0.0040	18.565	15.620	38.546
GR41-9	2.10	0.57	18.4062	15.6064	38.3704	0.0012	0.0011	0.0026	18.420	15.623	38.426
GR35-9	2.05	0.45	18.5088	15.6223	38.5196	0.0017	0.0014	0.0035	18.522	15.639	38.576

*Values corrected for internal fractionation using ^{203}Tl/^{205}Tl = 0.418922 and for external fractionation using nominal values of SRM981 of Baker *et al.* (2004).

samples (Bonev & Stampfli, 2009; Bonev, 2020). The range of Nd isotopes is consistent with the values of the oceanic crust developed in the seafloor and arc-related settings such as refractory mantle peridotite. The Pb isotope data also suggest a contribution of MORB mantle source. Thus, the boninitic–tholeiitic basalt to andesites and gabbros exhibits Nd and Pb isotopic chemistry that suggests contribution from depleted MORB-type mantle source in the magma generation (Fig. 2). The relatively narrow range of $\epsilon_{Nd}(t)$ and Pb isotope values indicates that the mantle source of the mafic lavas and gabbros was rather homogeneous, depleted MORB-type lithospheric mantle.

The range of Sr isotopes also supports a MORB-type mantle component in the source region, but in addition shows the enrichment process via crustal contamination, explaining the variations and high ^{87}Sr/^{86}Sr ratio in samples Dd2 and GR44-9. The dyke Dd2 shows a deep negative Ce anomaly that has been interpreted in favour of involvement of the sediments in the subduction zone (Bonev & Stampfli, 2009). We infer a contribution from continental crust to explain the elevated ^{87}Sr/^{86}Sr ratios (0.7071 and 0.7075) observed in these samples. The negative $\epsilon_{Nd}(t)$ value of sample GR44-9 suggests that more likely subducted sediments were involved in the magma genesis. The fact that sample Dd2 belongs to the fore-arc segment, and that both it and sample GR44-9 are based on ^{87}Sr/^{86}Sr values, might well demonstrate a contribution of sedimentary input into the fore-arc region of the subduction zone. We infer, therefore, the involvement of MORB reservoir in the mantle source region mixed with crustal component in the source mantle of subduction zone from the fore-arc to arc edifice.

Our results highlight coherent Nd–Sr–Pb isotopic ratios of the Evros ophiolite mafic rocks, indicating generation of magmas by partial melting of a MORB-source mantle. These isotopic data

https://doi.org/10.1017/S0016756822001285 Published online by Cambridge University Press

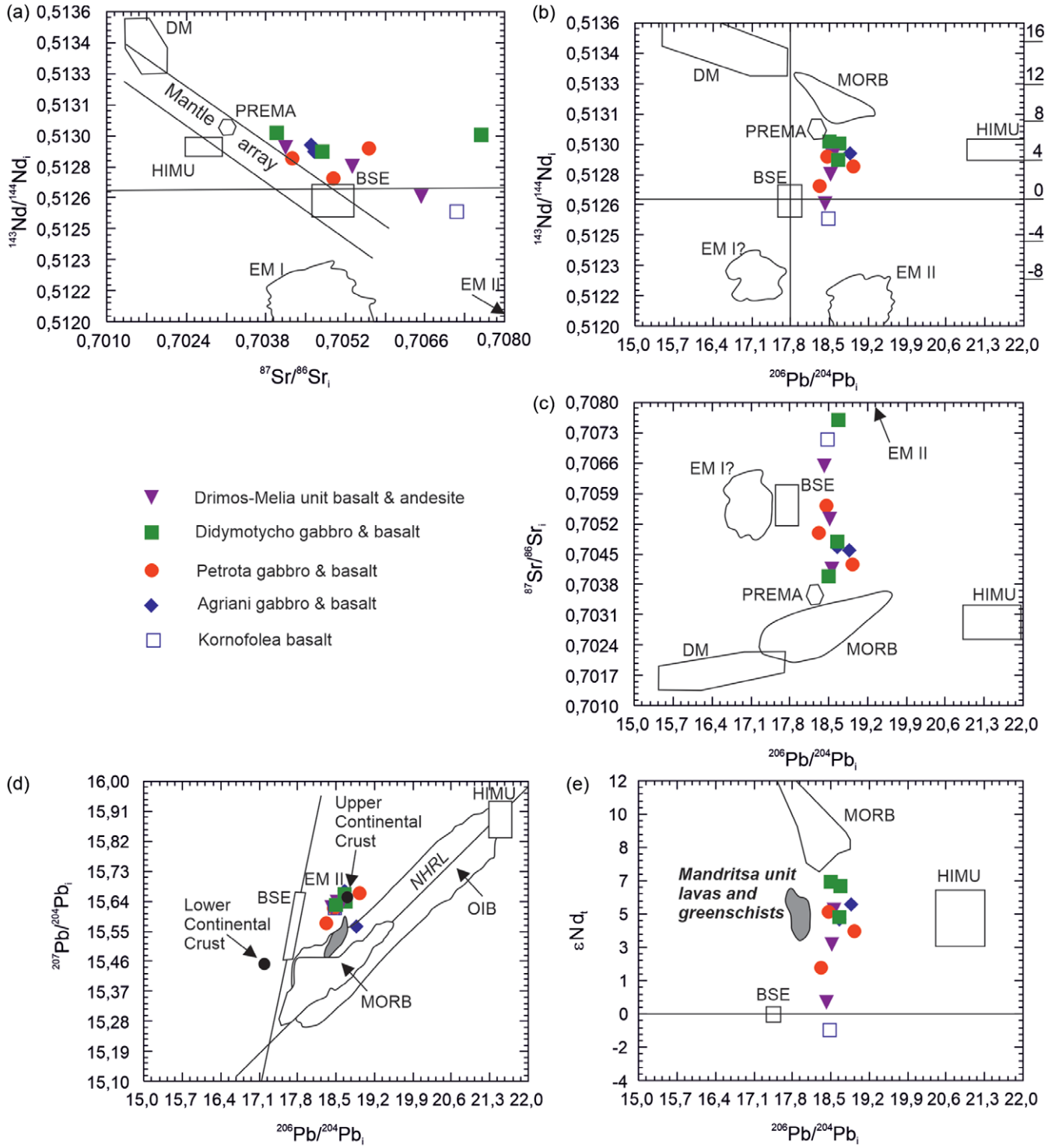

Fig. 2. (Colour online) Correlation diagrams for Nd–Sr–Pb isotopes of the Evros ophiolite mafic rocks. (a) $^{143}Nd/^{144}Nd$ vs $^{87}Sr/^{86}Sr$ diagram. DMM and EMI mantle reservoirs from Hart (1984). (b) $^{143}Nd/^{144}Nd$ vs $^{206}Pb/^{204}Pb$ diagram. (c) $^{87}Sr/^{86}Sr$ vs $^{206}Pb/^{204}Pb$ diagram. (d) $^{207}Pb/^{204}Pb$ vs $^{206}Pb/^{204}Pb$ diagram. The NHRL and the fields of reference mantle reservoirs are after Zindler & Hart (1986), and the fields of OIB and MORB from Rollinson (1993). (e) $\epsilon_{Nd}(t)$ vs $^{206}Pb/^{204}Pb$ diagram. Mantle reservoirs are after Zindler & Hart (1986).

indicate variable contamination of magmas by continental crust material and/or sediments entrained in the subduction zone (Fig. 3). These isotopic and compositional features are compatible with an intra-oceanic arc system represented by the Evros ophiolite in the Tethyan realm (Fig. 3), and are similar, for example, to the documented chemostratigraphy in some of the Pacific Ocean fore-arc–arc systems (Yu *et al.* 2020, 2022). Comparision of the Nd–Pb isotope results with analogous data from the Mandritsa unit mafic

https://doi.org/10.1017/S0016756822001285 Published online by Cambridge University Press

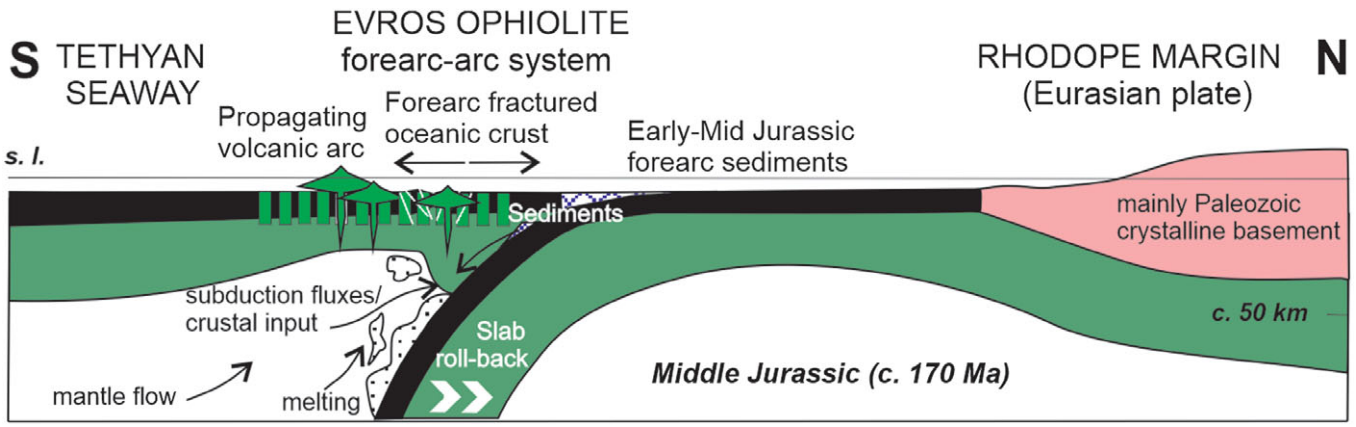

Fig. 3. (Colour online) Simplified model of the Evros ophiolite Middle Jurassic intra-oceanic tectonic setting in the Tethyan realm accounting for the mantle–crust interaction in the mantle wedge as derived from the Nd–Sr–Pb isotopic results.

rocks demonstrates region-wide similarity of the isotopic compositions, which in turn provides additional support for the supra-subduction zone origin for the Evros ophiolite in the eastern CRB. Overall, the Nd–Sr–Pb isotopes systematics revealed mantle–crust interaction caused by mantle wedge magmatic process in supra-subduction zone Evros ophiolite.

Acknowledgements. The support provided by the National Science Fund (Bulgaria) under contract KP-06-N54/5 is gratefully acknowledged. We thank Yildirim Dilek for careful reading and commenting on the manuscript, which helped us to improve the article.

References

Baker J, Peate D, Waight T and Meyzen C (2004) Pb isotopic analysis of standards and samples using a ^{207}Pb–^{204}Pb double spike and thallium to correct for mass bias with a double-focusing MC-ICPMS. *Chemical Geology* **211**, 275–303.

Biggazzi G, Del Moro A, Innocenti F, Kyriakopoulos K, Manetti P, Papadopoulos P, Norelliti P and Magganas A (1989) The magmatic intrusive complex of Petrota, west Thrace: age and geodynamic significance. *Geologica Rhodopica* **1**, 290–7.

Bonev N (2020) *Geology of the Eastern Circum-Rhodope Belt*. Sofia: University Press 'St. Kliment Ohridski', 240 pp. (in Bulgarian, with English summary).

Bonev N and Beccaletto L (2007) From syn- to post-orogenic Tertiary extension in the north Aegean region: constraints on the kinematics in the eastern Rhodope-Thrace, Bulgaria-Greece and the Biga Peninsula, northwest Turkey. In *The Geodynamics of the Aegean and Anatolia* (eds T Taymaz, Y Yilmaz and Y Dilek), pp. 113–42. Geological Society of London, Special Publication no. 291.

Bonev N, Burg J-P and Ivanov Z (2006) Structural evolution of an extensional gneiss dome: the Kesebir-Kardamos dome, E. Rhodope, Bulgaria-Greece. *International Journal of Earth Sciences* **95**, 318–40.

Bonev N and Filipov P (2018) From an ocean floor wrench zone origin to transpressional tectonic emplacement of the Sithonia ophiolite, eastern Vardar Suture Zone, northern Greece. *International Journal of Earth Sciences*, **107**, 1689–711.

Bonev N, Magganas A and Klain L (2010a) Regional geology and correlation of the eastern Circum-Rhodope Belt, Bulgaria-Greece. In *Proceedings XIX Congress Carpathian-Balkan Geological Association (CBGA), Special volume 100* (eds G Christofides, N Kantiranis, DS Kostopoulos and AA Chatzipetros), pp. 157–64. Scientific Annals, School of Geology, Aristotle University of Thessaloniki.

Bonev N, Marchev P, Moritz R and Collings D (2015a) Jurassic subduction zone tectonics of the Rhodope Massif in the Thrace region (NE Greece) as revealed by new U-Pb and ^{40}Ar/^{39}Ar geochronology of the Evros ophiolite and high-grade basement rocks. *Gondwana Research* **27**, 760–75.

Bonev N, Marchev P, Moritz R and Filipov P (2015b) Timing of igneous accretion, composition, and temporal relations of the Kassandra-Sithonia rift-spreading center within the eastern Vardar suture zone, Northern Greece: insights into Jurassic arc/back-arc systems evolution at the Eurasian plate margin. *International Journal of Earth Sciences* **104**, 1837–64.

Bonev N, Spikings R, Moritz R and Marchev P (2010b) The effect of early Alpine thrusting in late-stage extensional tectonics: evidence from the Kulidzhik nappe and the Pelevun extensional allochthon in the Rhodope Massif, Bulgaria. *Tectonophysics* **488**, 256–81.

Bonev NG and Stampfli GM (2003) New structural and petrologic data on Mesozoic schists in the Rhodope (Bulgaria): geodynamic implications. *Comptes Rendus Geosciences* **335**, 691–99.

Bonev N and Stampfli G (2005) Compositional diversity of the Evros ophiolite, Thrace, northeastern Greece: field occurrences, preliminary petrologic and geochemical data on plutonic sequence and tectonic implications. In *Proceedings of the Annual Conference of the Bulgarian Geological Society, 'Geosciences 2005'* (eds Y Yanev and R Nedyalkov), pp. 28–31. Sofia: Bulgarian Geological Society.

Bonev N and Stampfli G (2008) Petrology, geochemistry and geodynamic implications of Jurassic island arc magmatism as revealed by mafic volcanic rocks in the Mesozoic low-grade sequence, eastern Rhodope, Bulgaria. *Lithos* **100**, 210–33.

Bonev N and Stampfli G (2009) Gabbro, plagiogranite and associated dykes in the supra-subduction zone Evros ophiolites, NE Greece. *Geological Magazine* **146**, 71–92.

Bonev N and Stampfli G (2011) Alpine tectonic evolution of a Jurassic subduction-accretionary complex: deformation, kinematics and ^{40}Ar/^{39}Ar age constraints on the Mesozoic low-grade schists of the Circum-Rhodope Belt in the eastern Rhodope-Thrace region, Bulgaria-Greece. *Journal of Geodynamics* **52**, 143–67.

Burg J-P, Ricou L-E, Ivanov Z, Godfriaux I, Dimov D and Klain L (1996) Synmetamorphic nappe complex in the Rhodope Massif: structure and kinematics. *Terra Nova* **8**, 6–15.

Chiaradia M, Müntener O and Beate B (2011) Enriched basaltic andesites from mid-crustal fractional crystallization, recharge, and assimilation (Pilavo Volcano, Western Cordillera of Ecuador). *Journal of Petrology* **52**, 1107–41.

Christofides G, Pécskay Z, Elefteriadis G, Soldatos T and Koroneos A (2004) The Tertiary Evros volcanic rocks (Thrace, northeastern Greece): petrology and K/Ar geochronology. *Geologica Carpathica* **55**, 397–409.

Dilek Y and Furnes H (2011) Ophiolite genesis and global tectonics: geochemical and tectonic fingerprinting of ancient oceanic lithosphere. *Geological Society of America Bulletin* **123**, 387–411.

https://doi.org/10.1017/S0016756822001285 Published online by Cambridge University Press

Dimadis L and Nikolov T (1997) An ammonite find in the Makri unit (Berriasian, southeast Rhodopes, northeast Greece). *Comptes Rendus de l'Académie Bulgare des Sciences* **50**, 71–4.

Dimadis L, Papadopolous P, Goranov A and Encheva M (1996) First biostratigraphic evidence for the presence of Triassic at Melia (Western Thrace, Greece). *Geologica Balcanica* **26**, 37–40.

Ferrière J, Baumgartner PO and Chanier F (2016) The Maliac Ocean: the origin of Tethyan Hellenic ophiolites. *International Journal of Earth Sciences* **105**, 1941–63.

Hart SH (1984) A large-scale isotope anomaly in the Southern Hemisphere mantle. *Nature* **309**, 753–57.

Ivanova D, Bonev N and Chatalov A (2015) Biostratigraphy and tectonic significance of lowermost Cretaceous carbonate rocks of the Circum-Rhodope Belt (Chalkidiki Peninsula and Thrace region, NE Greece). *Cretaceous Research* **52**, 25–63.

Kauffmann G, Kockel F and Mollat H (1976) Notes on the stratigraphic and paleogeographic position of the Svoula formation in the Innermost Zone of the Hellenides (Northern Greece). *Bulletin de la Société Géologique de France* **18**, 225–30.

Koglin N, Reischmann T, Kostopoulos D, Matukov D and Sergeev S (2007) Zircon SHRIMP ages and the origin of ophiolitic rocks from the NE Aegean region, Greece. *Geophysical Research Abstracts* **9**, paper 06848.

Kopp KO (1965) Geologie Thrakiens III. Das Tertiär zwishen Rhodope und Evros. *Annales géologiques des pays Helléniques* **16**, 315–62.

Kopp KO (1969) Geologie Thrakiens VI: Der Coban Dag westlich von Alexandroupolis. *Geotektonische Forschungen* **31**, 97–116.

Magganas A, Sideris C and Kokkinakis A (1991) Marginal basin-volcanic arc origin of metabasic rocks of the Circum-Rhodope Belt, Thrace, Greece. *Mineralogy and Petrology* **44**, 235–52.

Magganas AC (2002) Constraints on the petrogenesis of Evros ophiolite extrusives, NE Greece. *Lithos* **65**, 165–82.

Maratos G and Andronopoulos B (1964) Nouvelles données sur l'âge des phyllites du Rhodope. *Bulletin of the Geological Society of Greece* **6**, 113–32.

McArthur JM, Howarth RJ and Bailey TR (2001) Strontium isotope stratigraphy: LOWESS version. 3: best fit for marine Sr-isotope curve for 0-509 Ma and accompanying look-up table for deriving numerical age. *The Journal of Geology* **109**, 155–70.

Meinhold G, Reischmann T, Kostopoulos D, Frei D and Larionov AN (2010) Mineral chemical and geochronological constraints on the age and provenance of the eastern Circum-Rhodope Belt low-grade metasedimentary rocks, NE Greece. *Sedimentary Geology* **229**, 207–33.

Papadopoulos P (1980) *Geological map of Greece, scale 1:50 000 sheet Maronia*. Xanthi: Institute of Geology and Mineral Exploration, Greece.

Papadopoulos P (1982) *Geological map of Greece, scale 1:50 000 sheet Ferai-Peplos-Ainos*. Xanthi: Institute of Geology and Mineral Exploration, Greece.

Papadopoulos P, Arvanitidis N and Zanas I (1989) Some preliminary geological aspects on the Makri unit (Phyllite series), Peri-Rhodope Zone. *Geologica Rhodopica* **1**, 34–42.

Papanikolau D (2009) Timing of tectonic emplacement of the ophiolites and terrane paleogeography in the Hellenides. *Lithos* **108**, 262–80.

Ricou L-E, Burg J-P, Godfriaux I and Ivanov Z (1998) The Rhodope and Vardar: the metamorphic and the olistostromic paired belts related to the Cretaceous subduction under Europe. *Geodinamica Acta* **11**, 285–309.

Robertson AHF (2002) Overview of the genesis and emplacement of Mesozoic ophiolites in the Eastern Mediterranean Tethyan region. *Lithos* **65**, 1–67.

Robertson AHF, Dixon JE, Brown S, Collins A, Morris A, Pickett E, Sharp I and Ustaömer T (1996) Alternative tectonic models for the Late Palaeozoic-Early Tertiary development of Tethys in the Eastern Mediterranean region. In *Paleomagnetism and Tectonics of the Mediterranean Region* (eds A Morris and DH Tarling), pp. 239–63. Geological Society of London, Special Publication no. 105.

Rollinson H (1993) *Using Geochemical Data: Evaluation, Presentation, Interpretation*. Tottenham: John Wiley and Sons, 343 pp.

Stampfli GM and Hochard C (2009) Plate tectonics of the Alpine realm. In *Ancient Orogens and Modern Analogues* (eds JB Murphy, JD Keppie and AJ Hynes), pp. 89–111. Geological Society of London, Special Publication, no. 327.

Tanaka T, Togashi S, Kamioka H, Amakawa H, Kagami H, Hamamoto T, Yuhara M, Orihashi Y, Yoneda S, Shimizu H, Kunimaru T, Takahashi K, Yanagi Y, Nakano T, Fujimaki H, Shinjo R, Asahara Y, Tanimizu M and Dragusanu C (2000) JNdi-1: a neodymium isotopic reference in consistency with La Jolla neodymium. *Chemical Geology* **168**, 279–81.

Trikkalinos JK (1955) Über das Alter der vortartiären Schichten des Gebietes von Alexandropoulis-Didymotichon, Westthrazien. *Annales Géologique des Pays Hellénique* **6**, 81–2.

Tsikouras B and Hatzipanagiotou K (1998) Petrogenetic evolution of an ophiolite fragment in an ensialic marginal basin, northern Aegean (Samothraki Island, Greece). *European Journal of Mineralogy* **10**, 551–67.

Yu M, Dilek Y, Yumul Jr GP, Yan Y, Dimalanta CB and Huang CY (2020) Slab-controlled elemental-isotopic enrichments during subduction initiation magmatism and variations in forearc chemostratigraphy. *Earth and Planetary Science Letters* **538**, 116217.

Yu M, Yumul Jr GP, Dilek Y, Yan Y and Huang CY (2022) Diking of various slab melts beneath forearc spreading center and age constraints of the subducted slab. *Earth and Planetary Science Letters* **579**, 117367.

Zindler A and Hart SR (1986) Chemical geodynamics. *Annual Reviews of Earth and Planetary Sciences* **14**, 493–571.

https://doi.org/10.1017/S0016756822001285 Published online by Cambridge University Press